Radiation-induced oxidative damage to the DNA-binding domain of the lactose repressor

Nathalie GILLARD*, Stephane GOFFINONT*, Corinne BURÉ*, Marie DAVIDKOVA†, Jean-Claude MAURIZOT*, Martine CADENE* and Melanie SPOTHEIM-MAURIZOT*[1]

*Centre de Biophysique Moléculaire, CNRS, rue C. Sadron, 45071 Orléans Cedex 2, France, and †Nuclear Physics Institute, Department of Radiation Dosimetry, Na Truhlarce 39/64, CZ-18086, Praha 8, Czech Republic

Understanding the cellular effects of radiation-induced oxidation requires the unravelling of key molecular events, particularly damage to proteins with important cellular functions. The *Escherichia coli* lactose operon is a classical model of gene regulation systems. Its functional mechanism involves the specific binding of a protein, the repressor, to a specific DNA sequence, the operator. We have shown previously that upon irradiation with γ-rays in solution, the repressor loses its ability to bind the operator. Water radiolysis generates hydroxyl radicals ($OH^{\cdot}$ radicals) which attack the protein. Damage of the repressor DNA-binding domain, called the headpiece, is most likely to be responsible of this loss of function. Using CD, fluorescence spectroscopy and a combination of proteolytic cleavage with MS, we have examined the state of the irradiated headpiece. CD measurements revealed a dose-dependent conformational change involving metastable intermediate states. Fluorescence measurements showed a gradual degradation of tyrosine residues. MS was used to count the number of oxidations in different regions of the headpiece and to narrow down the parts of the sequence bearing oxidized residues. By calculating the relative probabilities of reaction of each amino acid with $OH^{\cdot}$ radicals, we can predict the most probable oxidation targets. By comparing the experimental results with the predictions we conclude that Tyr^{7}, Tyr^{12}, Tyr^{17}, Met^{42} and Tyr^{47} are the most likely hotspots of oxidation. The loss of repressor function is thus correlated with chemical modifications and conformational changes of the headpiece.

Key words: ionizing radiation, lactose repressor, mass spectrometry, Monte Carlo simulation, protein oxidation, radiolytic attack.

INTRODUCTION

Exposure to ionizing radiation induces alterations in redox-sensitive metabolic processes, apoptosis, mutagenesis and carcinogenesis through very complex phenomena involving damage and repair of DNA, as well as damage to other cellular components. Damage to DNA is considered to be the critical event in the destructive effect of ionizing radiation, and therefore the type of DNA lesions, their distribution and their repair is well studied [1]. However, DNA accomplishes its biological function by interacting with other cellular components, mainly proteins involved in replication, transcription, the regulation of gene expression, chromatin remodelling and epigenetic control. The physical integrity of DNA is maintained by interaction with structural proteins as well as repair proteins that are capable of reversing stress or metabolism-driven oxidative DNA lesions. DNA-binding proteins protect DNA from attack by the products of water radiolysis, particularly from the most aggressive one, the oxidizing hydroxyl radical ($OH^{\cdot}$ radical). However, by interacting with the radicals, the proteins themselves get damaged to the point of losing function when exposed to doses of radiation above a system-dependent threshold. Protein damage has the potential to disrupt the function of DNA–protein complexes, leading to dramatic cellular effects. Moreover, the cell is endowed with DNA-repair mechanisms, whereas there are far fewer opportunities for remediation for damaged proteins.

Radiation-induced damage to proteins has been the object of far fewer studies than DNA damage until now. Moreover, the $OH^{\cdot}$ radical is also one of the main reactive oxygen species produced in cells upon oxidative stress. Protein oxidation induced by oxidative stress is known to be involved in aging, neurodegenerative processes and cardiovascular diseases [2]. Resistance to oxidation is a sought-after property for therapeutic proteins [3]. The similarities between protein oxidation induced by radiation and by oxidative stress broadens the scope of protein damage studies, especially in the light of the discovery of a growing number of epigenetic effects.

Protein exposure to ionizing radiations induces modifications of the side chains of amino acids and peptide chain breaks. Many of these lesions and their mechanisms of formation have been identified [4,5]. The amino acids with the highest reactivity toward $OH^{\cdot}$ radicals are cysteine, tryptophan, tyrosine, methionine and phenylalanine [6–8]. In a protein, the reactivity of amino acids is modulated by the accessibility of the residues to the $OH^{\cdot}$ radical. We have built a model of simulation of the radiolytic attack (RADACK) which takes into account both the chemical reactivity of each amino acid towards the diffusing $OH^{\cdot}$ radicals and the accessibility of the reactive sites [9–11]. RADACK can be used to calculate the probability of reaction of each residue with $OH^{\cdot}$ radical for proteins with known three-dimensional structure as determined by NMR or crystallography.

We have reported previously the radiation-induced dysfunction of several DNA–protein complexes: the *Escherichia coli* lactose operator–repressor complex, the complex between MC1, a DNA-structuring protein of the archaeon *Methanosarcina thermophila* and its specific DNA sequence, as well as the complex between a DNA bearing an analogue of an abasic site and the repair protein Fpg of *Lactococcus lactis*. When irradiated with γ-rays, the three

Abbreviations used: ESI–IT, electrospray ionization–ion trap; HTH, helix–turn–helix; MALDI–TOF, matrix-assisted laser-desorption ionization–time-of-flight; MS/MS, tandem MS; RADACK, radiolytic attack; TFA, trifluoroacetic acid.

[1] To whom correspondence should be addressed (email spotheim@cnrs-orleans.fr).

complexes studied are disrupted mainly due to protein damage. The irradiation of the free proteins induces the loss of their ability to bind DNA at even lower doses than those necessary to the disruption of the irradiated complexes owing to the protection of the proteins by the bound DNA [10,12–14].

After investigating the damage to DNA upon the irradiation of the *E. coli* lactose operator–repressor complex [15,16], we focus here on the damage of the protein.

The *E. coli* lactose repressor is a homotetrameric protein (monomer of 360 amino acids) organized into two dimers. It contains the following domains: the tetrameric core (formed by the C-terminal regions of the four monomers and containing amino acids 59–360) and four headpieces (each one being the N-terminal region of the monomer and containing amino acids 1–49) linked to the core by a hinge which is unfolded in the free state (amino acids 50–58). The headpiece contains three α helices (residues Leu^{6}–Ala^{13}, Tyr^{17}–Val^{24} and Ala^{32}–Leu^{45}) linked by loops. The first two helices form, together with their connecting loop, the HTH (helix–turn–helix) motif which interacts directly with the major groove of operator DNA. The second helix is called the recognition helix [17–19]. Both headpiece domains of a dimer can bind one operator DNA, and, in this case, the hinge becomes structured [20–22]. It should be noted that the headpiece does not contain any cysteine, tryptophan or phenylalanine residues.

Using a phenomenological model accounting for our experimental results, we have shown previously that a repressor ceases to bind DNA when both its dimers are inactivated by irradiation. Furthermore, each dimer is inactivated when at least one monomer is inactivated. Finally, one monomer is inactivated with as little as two radiation-induced instances of damage. We have also concluded that the two critical cases of damage may result from the oxidation of amino acids side chains, probably located in the headpieces, by $OH^{\cdot}$ radicals [13].

In the present study, we investigated in detail the state of an irradiated headpiece. The overall conformation and the modifications of amino acid side chains were examined using a combination of CD, fluorescence spectroscopy and MS. The damage observed experimentally is discussed in relation to the predictions of the RADACK model.

MATERIALS AND METHODS

Headpiece preparation

The DNA sequence coding for the headpiece was inserted in the pET24a(+) plasmid (Novagen) and the peptide was expressed in the BL21(DE3) overproducing strain of *E. coli* (Stratagene). After expression, cells were lysed by sonication in a lysis buffer (50 mM potassium phosphate buffer, pH 7.5, 250 mM NaCl, 1 mM EDTA, 1 mM PMSF, 5 mM 2-mercaptoethanol and 5 % glycerol) at a ratio of 6 g of cell/60 ml of buffer. After centrifugation at 17 000 ***g*** for 30 min, the supernatant was treated with ammonium sulfate and centrifuged under the same conditions. The resulting pellet was dissolved in 1 litre of SP0 buffer (50 mM phosphate buffer, pH 7.5, 1 mM PMSF, 5 mM 2-mercaptoethanol and 5 % glycerol). The extract was then loaded on to a cation-exchanging sulfopropyl column (HiLoad™ 16/10 SP Sepharose™ HP; Amersham Biosciences) equilibrated in SP1 buffer (50 mM phosphate buffer, pH 7.5, 100 mM NaCl, 1 mM PMSF, 5 mM 2-mercaptoethanol and 5 % glycerol). After washing with SP1 buffer, the protein was eluted with a SP1/SP2 gradient (SP2 buffer: 50 mM phosphate buffer, pH 7.5, 600 mM NaCl, 1 mM PMSF, 5 mM 2-mercaptoethanol and 5 % glycerol). The fractions containing the headpiece were then precipitated in 75 % ammonium sulfate. The protein pellet was dissolved in 4 ml of AcA buffer (25 mM Hepes, pH 7.5, 1 M NaCl, 5 mM 2-mercaptoethanol, 0.1 mM PMSF and 5 % glycerol) and loaded on to a gel-filtration column (Ultrogel® AcA 54). After elution with AcA buffer, the fractions containing the protein were precipitated by ammonium sulfate. The headpiece was finally stored at − 20 °C in a 1 M Tris/HCl, pH 7.45, 10 mM 1,4-dithiothreitol and 20 % glycerol buffer. Before use, headpiece aliquots were buffer-exchanged by elution on a Sephadex G-25 column. The final headpiece concentration was determined by spectrophotometric measurements, assuming that $\varepsilon_{280} = 4800\ M^{-1} \cdot cm^{-1}$.

Headpiece irradiation

Samples of headpiece solutions were contained in 1.5 ml polypropylene microtubes (Eppendorf). The irradiated volumes were typically 10–100 μl. The tubes were immersed in an ice bath and irradiated in a ^{137}Cs irradiator (IBL437, CisBio International) delivering 0.6 MeV γ-rays at a dose rate of $9\ Gy \cdot min^{-1}$. For CD and fluorescence measurements, the samples were irradiated directly in the spectrometer quartz cells. Dosimetry was performed using Fricke's chemical dosimeter.

Circular dichroism

The headpiece conformation was studied by CD with a JASCO J-810 dichrograph. The spectra, in the wavelength range 200–250 nm, were recorded in quartz cells of 2 mm pathlength. Irradiation and CD measurements were realized with samples of 29 μM in a 25 mM ammonium cacodylate buffer (pH 7.25).

Fluorescence measurements

Fluorescence emission spectroscopy was used to study damage to tyrosine residues and search for dityrosine formation. Emission spectra (excitation wavelength 275 nm for tyrosine study, 320 nm for dityrosine, and 5 nm bandwidth) were recorded in silica cells of 5 mm pathlength using a Jobin-Yvon Fluoromax 2 spectrofluorimeter (from 280 to 320 nm for tyrosine formation and from 360 to 490 nm for dityrosine formation). Irradiation and fluorescence measurements were obtained at a headpiece concentration of 29 μM in a 25 mM ammonium cacodylate buffer (pH 7.25).

Theoretical calculations: RADACK model

The stochastic simulation model RADACK [9–11] was applied for the determination of the probability of each residue to react with $OH^{\cdot}$ radicals. The calculation is based on the structure of the headpiece determined by NMR (PDB code 1LQC) [18]. Smoluchovski's spheres with radius proportional to the reactivities of the amino acids were placed on the reactive hydrogen atoms of all amino acids. All non-reactive atoms are represented by Van der Waals spheres. The relative probability of reaction between freely diffusing $OH^{\cdot}$ radicals and the amino acids of the headpiece was determined.

Proteolytic cleavage

The side-chain modifications were studied by a combination of proteolytic cleavage and MS. Samples of headpiece protein at a final concentration of 20 μM were digested with endoproteinase GluC (Roche) in a 25 mM ammonium cacodylate buffer, 10 mM $CaCl_2$, 5 mM DTT (dithiothreitol), 0.5 mM EDTA, 50 mM NaCl (pH 7.6) for 150 min, at 37 °C using an enzyme/headpiece ratio of 1:25 (w/w), and alternatively with endoproteinase ArgC (Roche) in the same buffer at 25 °C and in an enzyme/headpiece ratio of 1:10 (w/w).

Mass spectrometry

MALDI–TOF (matrix-assisted laser-desorption ionization–time-of-flight) analysis

The native and irradiated headpieces were analysed by MALDI–TOF MS without further purification. The whole protein was first analysed to follow global patterns of irradiation damage. The headpiece was characterized further after proteolysis to identify peptides bearing radiation-induced oxidations.

The sample stage was coated using the ultra-thin layer method [23]. A matrix solution of 33 % (v/v) acetonitrile saturated with α-cyano-4-hydroxycinnamic acid, and containing an internal standard mixture of bradykinin, neurotensin and insulin (average masses of 904.5, 1672.9 and 3494.6 Da respectively) was freshly prepared. Samples were diluted 20-fold with this matrix solution and a 0.5 μl aliquot was spotted on to the sample stage. As soon as matrix–analyte co-crystals formed to homogeneity, the excess solution was removed by vacuum aspiration. MALDI–TOF analysis (Autoflex, Bruker) was performed in linear mode with delayed extraction. The data were acquired from accumulation of 200 laser shots (N_2 laser, 337 nm) with external calibration in Flex Control software. Spectra were calibrated internally and further processed using Flex Analysis software (Bruker).

ESI–IT (electrospray ionization–ion trap) analysis

Samples of proteolysed headpiece were desalted on C_{18} ZipTip® (Millipore). The resin was washed with a 50 % acetonitrile solution and equilibrated with 0.1 % aqueous TFA (trifluoroacetic acid). The samples were acidified with 2 % methanoic (formic) acid and loaded on to the resin. The resin was washed with a 5 % methanol and 0.1 % TFA solution, and the peptides were eluted with a 70 % acetonitrile and 0.1 % methanoic acid solution. Desalted samples were diluted 5-fold further with the same solution and analysed by ESI–IT MS (Esquire HCT, Bruker). The peptide mixture was analysed in MS mode with external calibration, and appropriate peptide ions were selected for fragmentation with acquisition times of 6 min and a 2.5 Da isolation window. Tandem MS (MS/MS) spectra were processed further using Data Analysis software from Bruker.

RESULTS

CD study of the headpiece conformation

The headpiece was irradiated in the dose range 0–2000 Gy. For each dose, the CD spectrum was recorded from 200 to 250 nm at 4 °C. As shown in Figure 1, the CD intensity decreases upon irradiation and the maximum negative intensity is displaced toward shorter wavelengths. An isodichroic point is observed at 204 nm. The inset of Figure 1 shows the normalized variation of ellipticity at 220 nm.

Furthermore, the thermal stability of the peptide was assayed by performing denaturation–renaturation cycles. Non-irradiated or irradiated headpiece samples were thermally denatured and renatured in the cell of the dichrograph: from 4 °C, the temperature was raised to 74 °C with a 2 °C/min gradient, and then decreased at the same rate. The CD signal intensity was recorded at 220 nm every 0.2 °C. To determine the fraction of native headpiece at each temperature, the native and denatured states were defined as follows: the 4 °C conformation of the non-irradiated headpiece was considered to be the native one, and the 74 °C conformation to be the denatured one. Figure 2 shows the denaturation curves of a non-irradiated and a 700 Gy-irradiated sample. Whereas the denaturation of the non-irradiated headpiece was completely reversible, this was not the case for the irradiated protein. Indeed, only 50 % of the fraction of a 700 Gy-irradiated headpiece sample was structured before denaturation and this value falls to 30 % after the denaturation–renaturation cycle. Moreover, the thermal stability of the sample is lowered since the melting temperature decreases upon irradiation from 43.5 to 40 °C.

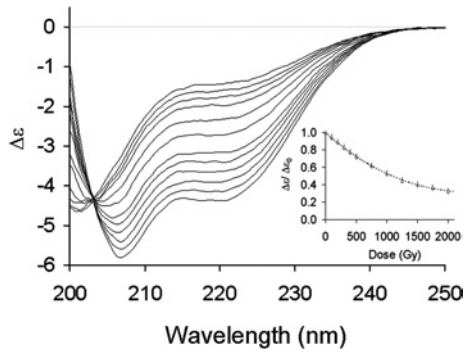

Figure 1 Secondary structure of the irradiated headpiece

CD spectra of the headpiece irradiated in the dose range 0–2000 Gy in a buffer containing 25 mM ammonium cacodylate, pH 7.25. The protein concentration was 29 μM. The inset shows the normalized variation of ellipticity at 220 nm.

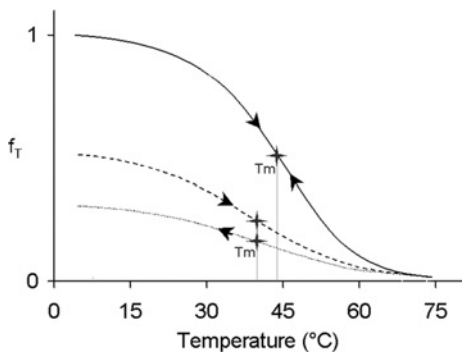

Figure 2 Thermal denaturation–renaturation cycle of intact and irradiated headpiece

Fraction of structured headpiece as a function of temperature during a denaturation–renaturation cycle, deduced from CD measurements. The cycle was performed for non-irradiated (solid line) and a 700 Gy-irradiated (broken lines) sample. $f_T = (\Delta\varepsilon_T - \Delta\varepsilon_d)/(\Delta\varepsilon_{nd} - \Delta\varepsilon_d)$ where $\Delta\varepsilon_T$, $\Delta\varepsilon_d$ and $\Delta\varepsilon_{nd}$ are the variations of ellipticity at 220 nm of the headpiece at temperature T, in the structured and in the denatured states respectively.

Fluorescence study of the state of the tyrosine residues

The destruction of the tyrosine side chains (residues 7, 12, 17 and 47) upon irradiation was followed by the decrease of intrinsic fluorescence of the peptide. In the absence of other aromatic residues, intrinsic fluorescence is due exclusively to tyrosine residues. The headpiece was irradiated in solution within the dose range 0–2000 Gy ($\lambda_{ex} = 275$ nm, and emission spectra recorded from 280 to 350 nm). As shown in Figure 3(A), the fluorescence of the headpiece decreases with increasing dose, without any change in the shape of the spectra. This decrease shows that tyrosine residues are degraded. Moreover, the evolution of the intrinsic fluorescence cannot be fitted with a simple exponential curve, which suggests that one or several tyrosine residues may be degraded faster than others.

Formation of dityrosines was observed by fluorescence measurements of the same samples using $\lambda_{ex} = 320$ nm. Emission

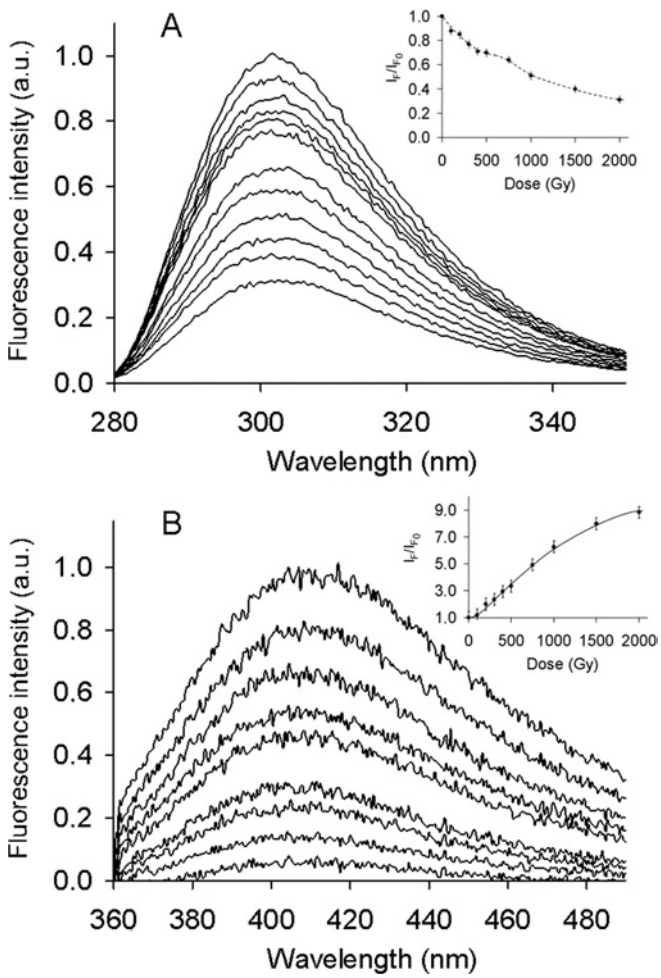

Figure 3 Tyrosine and dityrosine band fluorescence of the irradiated headpiece

(**A**) Fluorescence emission spectra of the headpiece as a function of dose (range 0–2000 Gy; $\lambda_{ex} = 275$ nm). The inset shows, in the emission band of tyrosine, the decrease of the fluorescence intensity as a function of dose. (**B**) Dityrosine band fluorescence emission spectra of the headpiece as a function of dose (range 0–2000 Gy; $\lambda_{ex} = 320$ nm). The inset shows, in the emission band of dityrosine, the increase of the fluorescence intensity compared with the dose. a.u., arbitrary units.

spectra were recorded from 360 to 490 nm. Figure 3(B) shows the increase of fluorescence intensity in the dityrosine emission band.

Calculated relative probabilities of the headpiece residues reaction with $OH^{\cdot}$ radicals

The RADACK model was used to determine the probability, for each residue, to react with $OH^{\cdot}$ radicals during irradiation. The location of the most reactive amino acids (tyrosine, methionine, histidine and arginine) in the three-dimensional structure (PDB code 1LQC) is shown in Figure 4(A), whereas in Figure 4(B), Smoluchowski's spheres are attributed to the reactive hydrogen atoms of the amino acids (RADACK representation). The largest spheres correspond to tyrosine residues. According to RADACK calculations, some residues have a higher probability than others of being damaged during radiolysis (Figure 4C). The difference of values for the four tyrosine residues reflects the influence of structure which modulates solvent accessibility and thus probability of reaction with $OH^{\cdot}$ radicals. The reactions of $OH^{\cdot}$ radicals with the protein have an 88 % relative probability of occurring on the side chains and only 12 % on the peptide backbone, because of the low accessibility of the reactive sites on the backbone in the compact structure of the headpiece.

Study of the irradiated headpiece by MS

MS (MALDI–TOF MS and ESI–IT MS) and tandem MS (ESI–IT MS/MS) experiments were performed to follow side-chain damage on the headpiece.

The headpiece was first irradiated within the dose range 0–1000 Gy and analysed by MALDI–TOF MS. The headpiece was analysed along with calibrants for accurate mass determination as shown in Figure 5(A). The headpiece mass was determined from the doubly charged protein ion is 6696.9 Da (theoretical average mass 6697.6 ± 0.7 Da). Figure 5(B) shows that protein irradiation leads to the appearance of new protein species with a mass difference of 16 or 14 Da. In linear mode, the resolution was insufficient to differentiate clearly between these two types of modifications. Moreover, sodium and potassium adducts can partially obscure multiple oxidations. However, oxidation events clearly follow a dose-dependant relationship: at 200 Gy, protein species with up to three events are observed, whereas at least five oxidation events are visible at 500 Gy. Each additional modification decreases the intensity of individual peaks by widening the distribution of oxidized species. Thus, at 1000 Gy, peaks are no longer resolved. The mass spectra do not show evidence of peptide backbone breakage.

Analysis of the whole headpiece does not allow for the identification of individual oxidized residues. In order to better localize the oxidation sites, the irradiated headpiece samples were proteolysed. We used either endoproteinase ArgC, which cleaves on the carboxylic side of arginine, or endoproteinase GluC, which cleaves on the carboxylic side of glutamic acid and in some conditions, aspartic acid residues. The cleavage products were analysed by MALDI–TOF MS (Figure 6). No uncleaved headpiece is detectable with either enzyme at 150 min of proteolysis (mass range not shown). However, some sites are only partially cleaved, such as Arg^{35} in the Val^{23}–Arg^{51} peptide (Figure 6, bottom panel). Cleavage at Asp^{8} with endoproteinase GluC is not observed. The C-terminal peptide (theoretical mass 1029.2 Da) is not detected after ArgC cleavage. Three oxidations are observed in the Val^{23}–Arg^{51} peptide, while no oxidation appears in Val^{23}–Arg^{35}. In fact, with the exception of the aforementioned peptide, all detected peptides bear one or more oxidations, as is evident from the presence of protein species with mass differences in multiples of 16 Da. Thus sites of oxidation seem dispersed throughout the sequence.

To localize damage on the sequence more precisely, MS/MS in an ion trap was performed. Peptide fragmentation along the peptide backbone may allow for the identification and localization of amino acid side-chain modifications. A headpiece sample was irradiated at a dose of 500 Gy and cleaved with endoproteinase ArgC. The sample was then desalted and analysed by ESI–IT MS. Several ions corresponding to mono-oxidized peptides were selected for fragmentation. The mono-oxidized peptides corresponding to sequences Met^{1}–Arg^{22} and Val^{23}–Arg^{51} produced useful fragmentation information with respect to oxidation (Figure 7). Ions are annotated following the Roepstorff–Fohlmann–Biemann nomenclature [24].

Fragmentation mainly occurs at the amide bond and leads to b_n (charge carried by the N-terminal end) and y_n (charge carried by the C-terminal end) ions. In the case of the Met^{1}–Arg^{22} peptide, both oxidized and non-oxidized b_{12} ions are observed. This shows that the oxidation can be borne by a residue located in the Met^{1}–Tyr^{12} or in the Ala^{13}–Arg^{22} region respectively. From this ion pair

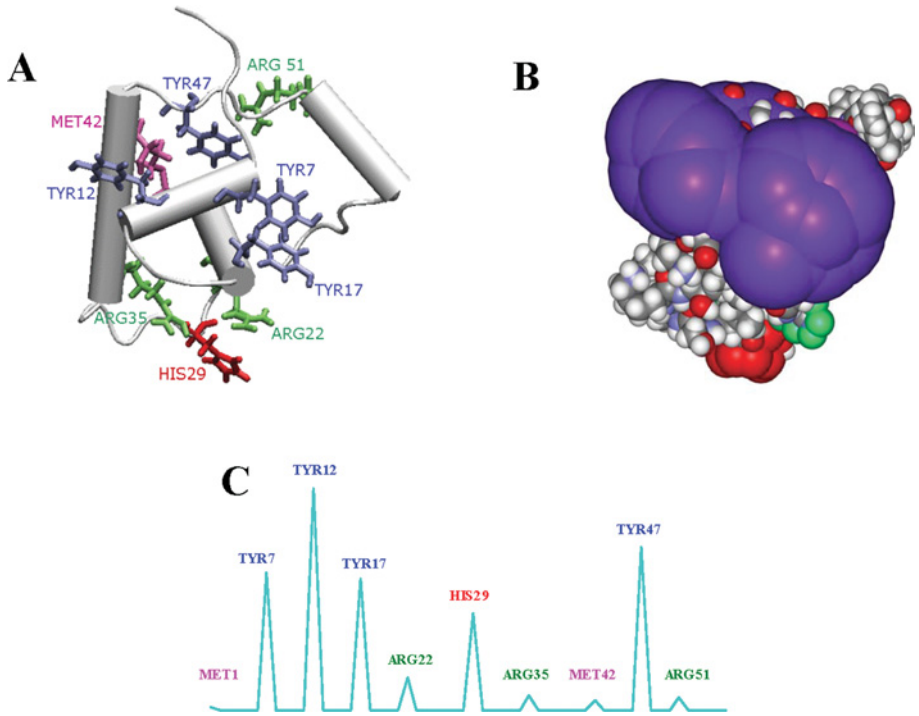

Figure 4 RADACK prediction of the damage sites

Probability of reaction of headpiece amino acids with $OH^{\cdot}$ radicals as calculated with the RADACK model using the NMR-based structure available in the PDB (accession code 1LQC) [18]. (**A**) Location of the most reactive amino acids in the headpiece. (**B**) RADACK representation of the headpiece with Smoluchowski's spheres on the reactive atoms (the headpiece position and the colours used for the amino acids are the same as in **A**). (**C**) Calculated relative probabilities of reaction of each amino acid with $OH^{\cdot}$ radicals.

and other pairs of oxidized/non-oxidized fragment ions, we can deduce that the observed mono-oxidized ion corresponds to a mixture of peptides. Moreover, for the Met^{1}–Arg^{22} peptide, a series of internal fragments starting at Pro^{3} and Thr^{5} are also observed (Table 1). The internal fragment series is informative as it shows with certainty that there is one oxidation in the Tyr^{12}–Ser^{16} region. The oxidized b series (Figure 7A) shows at least one oxidation in the Met^{1}–Glu^{11} region. The oxidized y series shows an oxidation in the Ala^{13}–Arg^{22} region. Interestingly, the oxidized to non-oxidized y ion intensity ratio decreases strongly after Tyr^{12}, while the oxidized to non-oxidized b ion intensity ratio increases beyond Glu^{11}. These observations reinforce the notion that, while different mono-oxidized species are present, a peptide oxidized at Tyr^{12} might significantly contribute to the overall ion intensity.

In addition to +16 Da fragments, a number of low-intensity +14 Da b ions (b_{11}–b_{21}) and a +14 Da y_{11} ion were observed. For the sake of clarity, these were not annotated on spectra or sequences. For fragments of the Val^{23}–Arg^{51} peptide, the oxidized y series localizes one oxidation in the Leu^{45}–Arg^{51} region. The oxidized b_{38} and b_{42}–b_{48} ions indicate possible oxidation in the Val^{23}–Glu^{44} region, while only non-oxidized b ions appear in the Val^{23}–Glu^{36} region. Together, these results suggest one probable oxidation in the Glu^{36}–Glu^{44} region. Moreover, the oxidized to non-oxidized b ion intensity ratio increases beyond Glu^{44}, which confirms the presence of at least one other major oxidation site in the Leu^{45}–Arg^{51} region.

DISCUSSION

Gene expression is a very finely regulated process. In the case of the lactose operon, binding of the repressor to the operator blocks the expression of three enzymes involved in lactose metabolism (β-galactosidase, lactose permease and thiogalactoside transacetylase). Only ten copies of the repressor protein are present per wild-type bacterial cell [25]. Consequently, any alteration to the repressor that triggers a loss of binding ability can have direct consequences on the expression of operon proteins. Having investigated the damage to operon DNA [15,16] and the effect of radiation on the function of the repressor [12], we focus here on the damage to the protein.

The damage of the repressor headpiece, the repressor DNA-binding domain, is the most likely cause of the radiation-induced loss of repressor-operator recognition. We have examined here its degradation using a combination of techniques: CD, fluorescence spectroscopy, MS and Monte Carlo simulation.

Figure 1 shows that the irradiation of the headpiece causes a decrease of the CD intensity and a shift of the maximum negative intensity to shorter wavelengths. This proves a partial loss of the helical structure of the protein as a result of irradiation. This effect on the structure of the DNA-binding domain of the repressor can contribute to the loss of its ability to bind DNA.

It was shown previously that the denaturation of the repressor headpiece by heat or by addition of increasing concentration of urea is reversible [26–28]. We have studied the thermal denaturation of the irradiated headpiece. As shown in Figure 2, the thermal denaturation of the control non-irradiated headpiece up to 74 °C is completely reversible. For the 700 Gy-irradiated headpiece, the fraction of structured headpiece at 4 °C is lower than that of the non-irradiated headpiece (only 50 % of the headpiece has a native-like structure). Moreover, after a denaturation–renaturation cycle, the protein does not recover its original conformation, since only 30 % of the headpiece is in a native state after cooling. Consequently, the thermal cycle results in an additional loss of structure of the irradiated headpiece. One explanation could be

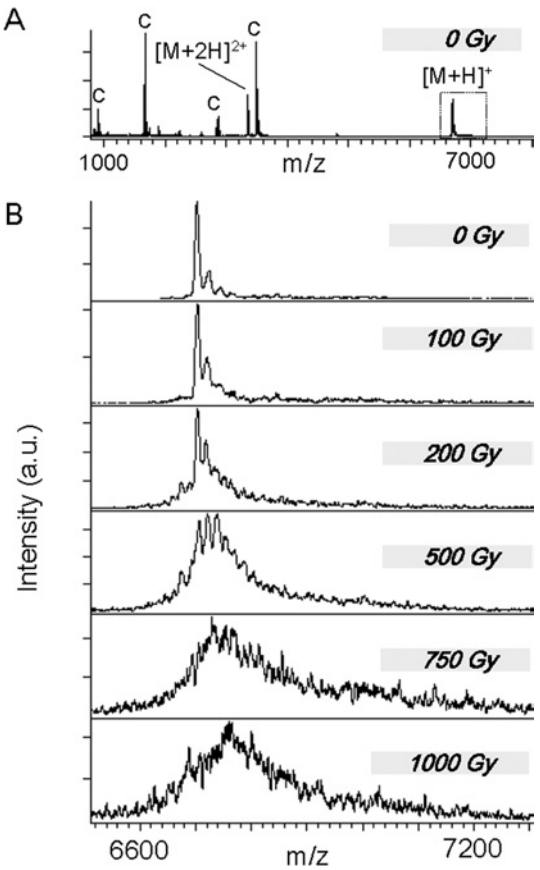

Figure 5 Oxidation of the whole headpiece

(**A**) MALDI–TOF spectrum of the non-irradiated headpiece analysed with a set of calibrants (c). (**B**) MALDI–TOF spectrum of irradiated samples of headpiece (29 μM in 25 mM ammonium cacodylate buffer, pH 7.25) in the dose range 0–1000 Gy. a.u., arbitrary units.

that every radiation-induced lesion does not lead to unfolding at 4 °C and therefore some regions remain in a native-like metastable state. Heating of the headpiece brings these regions over an energy barrier and induces their unfolding. During cooling of the completely denatured headpiece, the energy barrier prevents these regions from recovering their initial structure.

The observed decrease of melting temperature upon irradiation is also consistent with the radiation-induced lesions leading to a partially unfolded protein.

According to RADACK calculations, all four tyrosine residues (Tyr^{7}, Tyr^{12}, Tyr^{17} and Tyr^{47}) of the headpiece present a high probability of reaction with $OH^{\cdot}$ radicals and, consequently, are prone to damage upon irradiation We could easily follow their degradation by fluorescence emission spectroscopy since the headpiece does not bear any tryptophan or phenylalanine residues and thus the intrinsic fluorescence of the protein is due exclusively to the tyrosine fluorescence. As shown in Figure 3, tyrosine residues are indeed destroyed upon irradiation. Degradation of tyrosine can lead to the formation of dityrosine and dopa, each of them emitting fluorescence [29–31]. The possible formation of dopa could not be followed because its spectrum would be hidden by that of native tyrosine, but dityrosine formation was observed. The inset of Figure 3(A) shows that the decrease of tyrosine fluorescence intensity does not fit a simple exponential curve. This means that the degradation rates of the four tyrosine residues are not the same and thus one or several residues might be damaged before the other ones. The production of dityrosine follows a sigmoidal curve (Figure 3B). By using molecular modelling, we have shown previously that the formation of dityrosine between Tyr^{7} and Tyr^{17} (the closest to each other in the three-dimensional structure of the headpiece and belonging to the two helices of the HTH recognition motif) energetically disfavours the operator–headpiece complex [32]. However, the presence of the dityrosine adducts revealed by the fluorescence measurements was not observed in MALDI–TOF experiments. This could be explained by the presence of only a small proportion of dityrosine and of a high proportion of dityrosine-like fluorescence, such as the relatively abundant (but chemically unidentified) species reported for irradiated RNase and lysozyme (accounting for 84 % and 98 % of the fluorescence respectively) [31].

RADACK calculation shows that not only tyrosine, but also some other amino acids have a high probability of reacting with $OH^{\cdot}$ radicals. MS was used to search for direct evidence of modification of all residues of the headpiece.

While MALDI–TOF analysis of intact compared with oxidized protein is only semi-quantitative under our conditions, we can infer that at least 10–15 % of the protein bears one or more oxidations at 100 Gy (Figures 5 and 6). According to our previous results and calculations under single-hit statistics conditions [15,33], 100 Gy are necessary to induce one or more strand breaks in 4 % of a DNA fragment of the size of the operator sequence (20 bp). Since the global number of instances of damage (strand breaks and base damage) is 3-fold that of strand breaks, approx. 12 % of the binding sequence will be damaged when DNA is irradiated with 100 Gy. Both partners thus bear a similar number of damage cases. However, the effect on binding seems different: at this dose, damage to the repressor affects complex formation directly, whereas damage to operator DNA has no effect [12]. A quantitative comparison is nevertheless not straightforward. Not only will damage to the headpiece lead to the destruction of the complex, but damage to the other part of the repressor (known as the core) may also contribute. It is known that binding of isopropyl β-D-thiogalactoside to the core changes the headpiece spatial orientation and thus hinders repressor–operator binding. Through similar allosteric effects, radiation-induced lesions to the core can affect headpiece binding to DNA, leading to an even greater sensitivity of the whole repressor to oxidation compared with the headpiece alone.

The study of the whole irradiated headpiece using MALDI–TOF shows that several side chains are oxidized upon irradiation. Proteolysis of the irradiated headpiece reveals the oxidized regions of the protein, while MS/MS analysis narrows them down.

By comparing the experimental MS results with RADACK prediction, we can pinpoint the most likely hotspots of radiation-induced damage in the headpiece. The oxidation observed in the Met^{1}–Glu^{11} region may correspond either to damage to Met^{1} or to Tyr^{7}. According to RADACK, the probability of damage of Tyr^{7} is much higher than that of Met^{1}. The oxidation in the Tyr^{12}–Ser^{16} region points towards damage of Tyr^{12}. The oxidation in the Ala^{13}–Arg^{22} region may correspond to the oxidation of Tyr^{17}. The oxidation of Val^{23}–Glu^{44}, without any oxidation in Val^{23}–Glu^{36}, is consistent with an oxidation of Met^{42}. In the Leu^{45}–Arg^{51} region, although Arg^{51} may contribute, according to RADACK, the strongest oxidation is likely to be localized at Tyr^{47}. In the Val^{23}–Arg^{51} peptide, two of the three observed oxidations can thus be due to oxidation of Met^{42} and Tyr^{47}. The third oxidized residue can be His^{29}, Arg^{35} or Arg^{51}. No positive evidence is available to unambiguously decide between these three possibilities. Table 2 summarizes the conclusions of the discussion of MS data in the light of RADACK predictions.

The identification of tyrosine residues as the most probable hotspots of oxidation is consistent with the loss of intact tyrosine

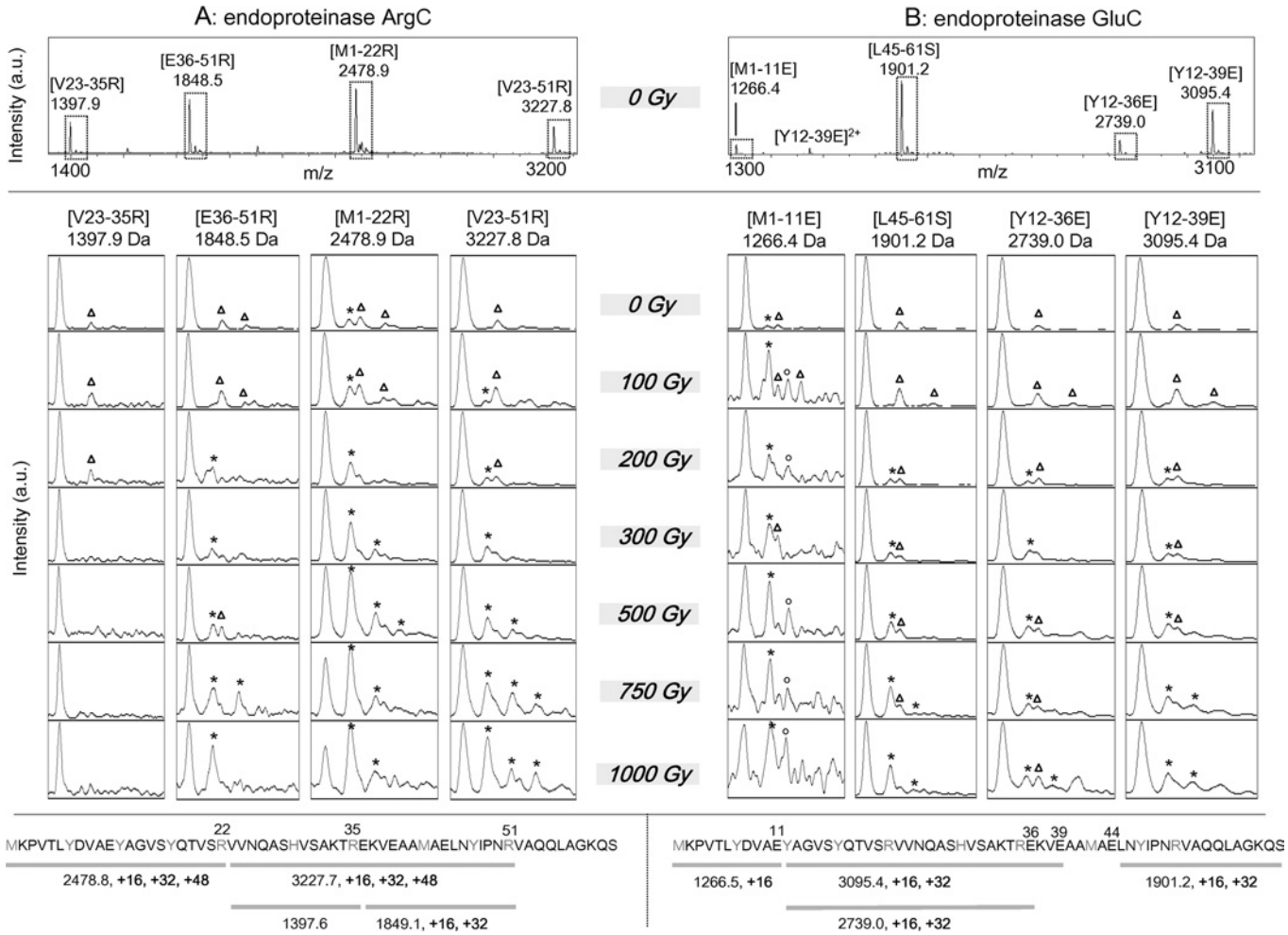

Figure 6 Oxidation of proteolytic peptides of the irradiated headpiece

Top panels: MALDI–TOF spectra of the non-irradiated headpiece proteolysed by endoproteinase ArgC (**A**) or GluC (**B**). Middle panels: 80 Da spectrum windows on proteolytic peptides of irradiated headpiece (0–1000 Gy). Oxidized species are marked with an asterisk, Δ indicates Na^+ and/or K^+ adducts. The species marked ○ is unidentified (1295.4 Da). Bottom panels: Summary of oxidations observed by MALDI–TOF. The residues that were shown by RADACK calculation as having the greatest probabilities to react with $OH^{\cdot}$ radicals are shown in grey in the sequence. Potential target residues for proteolysis bear numbers. The theoretical average mass of singly charged intact peptides is indicated, as well as observed oxidations. V23-35R, Val^{23}–Arg^{35}; E36-51R, Glu^{36}–Arg^{51}; M1-22R, Met^{1}–Arg^{22}; V23-51R, Val^{23}–Arg^{51}; M1-11E, Met^{1}–Glu^{11}; L45-61S, Leu^{45}–Ser^{61}; Y12-36E, Tyr^{12}–Glu^{36}; Y12-39E, Tyr^{12}–Glu^{39}. a.u., arbitrary units.

residues observed by fluorescence. Moreover, given the location of Tyr^{7}, Tyr^{12} and Tyr^{17} in the two helices of the HTH motif, one can easily understand the radiation-induced loss of helical structure observed by CD. The loss of binding ability of the repressor to operator DNA upon irradiation is thus probably based on the loss of recognition function of the headpiece HTH motif.

Until now, radiation-induced damage of proteins has been successfully used as a tool for probing protein structure and interactions in cases where three-dimensional structure of the protein or of protein complexes is not available [34–36]. In the present study, we have shown that a combination of analytical methods can be used to determine the radiation-induced damage of a DNA-binding protein with a known structure.

Our results reveal alterations of a protein upon irradiation and show that its loss of function is correlated with conformational changes and chemical modifications. The damage to the protein is one of the initial radiation-induced events, which under the influence of the cellular environment and, after processing by cellular mechanisms, are involved in the deleterious effects of ionizing radiation *in vivo*.

In the cell, a DNA-binding protein is not only in the presence of its partner DNA sequence, but also in the presence of many other molecules. These can act as radioprotectors by scavenging $OH^{\cdot}$ radicals, by shielding the target residues, and by chemical repair. They can, however, also act as radiosensitizers. All molecules, even radioprotectors, are attacked by $OH^{\cdot}$ radicals, and reactive radicals are formed on them. These secondary radicals will inflict additional damage on the protein [37]. Thus, for a dose where an isolated protein in solution is only slightly damaged, *in vivo* the same protein could sustain much more damage if the radiosensitization overcomes the protection. The overall effect is the sum of all radioprotective and radiosensitizing effects. In addition, protein oxidation leads to reduced proteasome-mediated degradation, accumulation of unfolded protein and a number of other phenomena which contribute to amplify the effect of the initial damage at the cellular level.

Interestingly, in spite of the complexity of the cellular environment, doses inducing measurable damage to the repressor headpiece in our *in vitro* study are in the same range as those affecting whole *E. coli* cell survival. For instance, a dose of 100 Gy

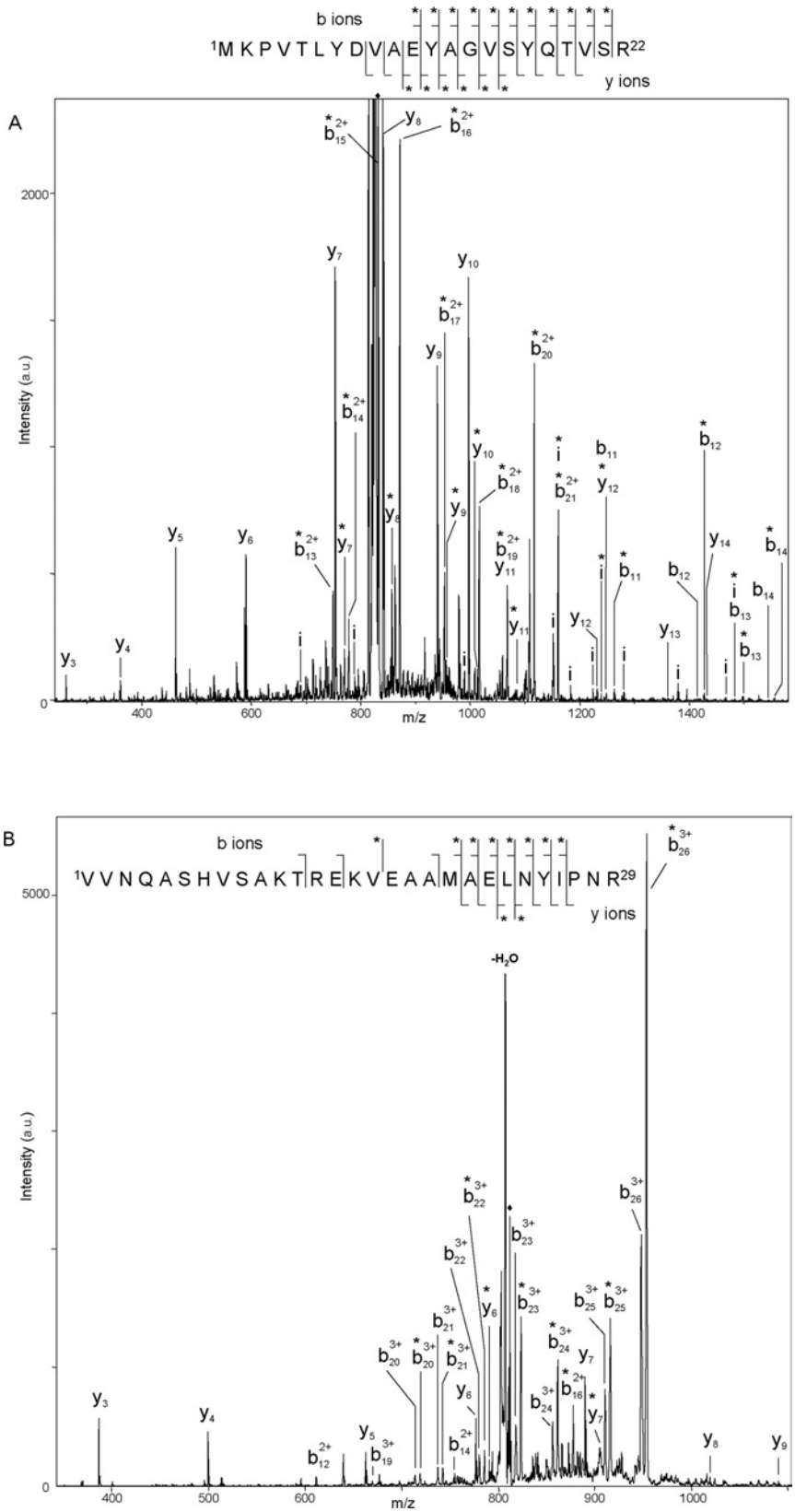

Figure 7 Localization of oxidations in irradiated headpiece peptides

Ion-trap fragmentation of mono-oxidized ArgC-cleavage peptides of the headpiece irradiated at 500 Gy. ESI–IT MS/MS spectra of (**A**) triply charged Met^{1}–Arg^{22} peptide, precursor *m/z* 832.2 Da (for the sake of clarity, the four most intense ions are left off-scale), and (**B**) quadruply charged Val^{23}–Arg^{51} peptide, precursor *m/z* 811.7 Da. Precursor ions are indicated with ◆. Spectra annotations reflect b_n and y_n ions, as well as internal ions labelled 'i'. Oxidized species are marked with an asterisk (b_n* and y_n* ions). The sequence is annotated once for each fragmentation site irrespective of the number of observed charge states for the fragment. For clarity, internal ions were not reported on the sequence and are listed in Table 1. a.u., arbitrary units.

Table 1 Oxidation state of internal fragments of mono-oxidized Met[1]–Arg[22] peptide observed by ESI–IT MS/MS

Fragment sequence	Without oxidation	Oxidized
P^3VTLYDVAEYAGVS^{16}	Yes	Yes
P^3VTLYDVAEYAGV^{15}	Yes	
P^3VTLYDVAEYAG^{14}	Yes	
P^3VTLYDVAEYA^{13}	Yes	Yes
P^3VTLYDVAEY^{12}	Yes	Yes
P^3VTLYDVAE^{11}	Yes	
P^3VTLYDV^{9}	Yes	
P^3VTLYD^{8}	Yes	
PV^5TLYDVAEYAGVS^{16}	Yes	

Table 2 Hotspots of radiolytic oxidation as deduced from a combination of MS and RADACK data

Headpiece region	Number of oxidations	Most probable hotspot
Met[1]–Glu[11]	1	Tyr[7]
Tyr[12]–Ser[16]	1	Tyr[12]
Ala[13]–Arg[22]	1	Tyr[17]
Lys[37]–Glu[44]	1	Met[42]
Leu[45]–Arg[51]	1	Tyr[47]

that induces the oxidation of approx. 10 % of the headpiece reduces the survival of wild-type *E. coli* by 10–20 % [38]. While we cannot conclude a direct relationship between the damage to the repressor molecule and the reduced survival of *E. coli* because of the complexity of the *in vivo* system, the idea that dysfunction of the lactose operon possibly contributes to the fitness or viability of the bacterium is intriguing.

In summary, upon irradiation, the lactose repressor loses its ability to bind the operator DNA. This is most probably due to damage to its DNA-binding domain, the headpiece. We have shown here that this domain undergoes a radiation-induced conformational change due to the damage (mainly oxidation) of amino acids. At 4 °C, some regions lose their helical structure, whereas others are in a metastable state. The oxidation occurs gradually with increasing dose, starting with the amino acids presenting the highest accessibility and the highest reactivity towards $OH^{\cdot}$ radicals. By combining the experimental results with RADACK prediction, we conclude that Tyr[7], Tyr[12], Tyr[17], Met[42] and Tyr[47] are the most likely hotspots of oxidation. Our results shed light on the modifications of a protein upon irradiation and show that chemical modifications and conformational changes are correlated with the radiation-induced loss of its function. This result is relevant for the understanding of cellular effects of ionizing radiation because protein damage is one of the multiple radiation-induced primary events that, under the influence of the cellular environment and after processing by cellular mechanisms, are involved in the deleterious effects of ionizing radiation *in vivo*.

This work was supported by a grant from Electricité de France (EDF), by a grant from Association pour la Recherche contre le Cancer (ARC), by the European COST (European Cooperation in the field of Scientific and Technical Research) Action 'Radiation damage in biomolecular systems' and by the bilateral Czech–French programme of scientific collaboration Barrande. M.C. is grateful to the CNRS for the award of an ATIP (Action Thématique Incitative sur Programme) grant.

REFERENCES

1 Cadet, J., Douki, T., Gasparutto, D. and Ravanat, J.-L. (2003) Oxidative damage to DNA: formation, measurement and biochemical features. Mutat. Res. **531**, 5–23
2 Fu, S., Davies, M. J., Stocker, R. and Dean, R. T. (1998) Evidence for roles of radicals in protein oxidation in advanced human atherosclerotic plaque. Biochem. J. **333**, 519–525
3 Brillard-Bourdet, M., Hamdaoui, A., Hajjar, E., Boudier, C., Reuter, N., Ehret-Sabatier, L., Bieth, J. G. and Gauthier, F. (2006) A novel locust (*Schistocerca gregaria*) serine protease inhibitor with a high affinity for neutrophil elastase. Biochem. J. **400**, 467–476
4 Garrison, W. M. (1987) Reaction mechanisms in the radiolysis of peptides, polypeptides, and proteins. Chem. Rev. **87**, 381–398
5 Stadtman, E. R. (1993) Oxidation of free amino acids and amino acid residues in protein by radiolysis and by metal-catalysed reactions. Annu. Rev. Biochem. **62**, 797–821
6 Buxton, G. V., Greenstock, C. L., Helman, W. P. and Ross, A. B. (1988) Critical review of rate constants for reactions of hydrated electrons, hydrogen atoms and hydroxyl radicals ($^{\cdot}OH$-$O^{\cdot -}$) in aqueous solution. J. Phys. Chem. Ref. Data **17**, 513–886
7 Finley, E. L., Dillon, J., Crouch, R. K. and Schey, K. L. (1998) Radiolysis-induced oxidation of bovine γ-crystallin. Photochem. Photobiol. **68**, 9–15
8 Audette, M., Blouquit, Y. and Houée-Lévin, C. (2000) Oxidative dimerization of protein: role of tyrosine accessibility. Arch. Biochem. Biophys. **376**, 217–220
9 Begusova, M., Spotheim-Maurizot, M., Sy, D., Michalik, V. and Charlier, M. (2001) RADACK, a stochastic simulation of hydroxyl radical attack to DNA. J. Biomol. Struct. Dyn. **19**, 141–158
10 Gillard, N., Begusova, M., Castaing, B. and Spotheim-Maurizot, M. (2004) Radiation affects binding of Fpg repair protein to an abasic site containing DNA. Radiat. Res. **162**, 566–571
11 Begusova, M., Gillard, N., Sy, D., Castaing, B., Charlier, M. and Spotheim-Maurizot, M. (2005) Radiolysis of DNA-protein complexes. Radiat. Phys. Chem. **72**, 265–270
12 Eon, S., Culard, F., Sy, D., Charlier, M. and Spotheim-Maurizot, M. (2001) Radiation disrupts protein–DNA complexes through damage to the protein: the *lac* repressor–operator system. Radiat. Res. **156**, 110–117
13 Charlier, M., Eon, S., Sèche, E., Bouffard, S., Culard, F. and Spotheim-Maurizot, M. (2002) Radiolysis of *lac* repressor by γ rays and heavy ions: a two hits model for protein inactivation. Biophys. J. **82**, 2373–2382
14 Culard, F., Gervais, A., de Vuyst, G., Spotheim-Maurizot, M. and Charlier, M. (2003) Response of a DNA-binding protein to radiation-induced oxidative stress. J. Mol. Biol. **328**, 1185–1195
15 Franchet-Beuzit, J., Spotheim-Maurizot, M., Sabattier, R., Blazy-Baudras, B. and Charlier, M. (1993) Radiolytic footprinting: β rays, γ photons and fast neutrons probe DNA–protein interactions. Biochemistry **32**, 2104–2110
16 Begusova, M., Eon, S., Culard, F., Charlier, M. and Spotheim-Maurizot, M. (2001) Radiosensitivity of DNA in a specific protein–DNA complex: the *lac* repressor–*lac* operator complex. Int. J. Radiat. Biol. **77**, 645–654
17 Kalodimos, C. G., Folkers, G. E., Boelens, R. and Kaptein, R. (2001) Strong DNA binding by covalently linked dimeric *Lac* headpiece: evidence for the crucial role of the hinge helices. Proc. Natl. Acad. Sci. U.S.A. **98**, 6039–6044
18 Kalodimos, C. G., Bonvin, A. M., Salinas, R. K., Wechselberger, R., Boelens, R. and Kaptein, R. (2002) Plasticity in protein–DNA recognition: *lac* repressor interacts with its natural operator 01 through alternative conformations of its DNA-binding domain. EMBO J. **21**, 2866–2876
19 Kalodimos, C. G., Boelens, R. and Kaptein, R. (2002) A residue-specific view of the association and dissociation pathway in protein–DNA recognition. Nat. Struct. Biol. **9**, 193–197
20 Spronk, C. A., Slijper, M., van Boom, J. H., Kaptein, R. and Boelens, R. (1996) Formation of the hinge helix in the *lac* repressor is induced upon binding to the *lac* operator. Nat. Struct. Biol. **3**, 916–919
21 Chuprina, V. P., Rullmann, J. A., Lamerichs, R. M., van Boom, J. H., Boelens, R. and Kaptein, R. (1993) Structure of the complex of *lac* repressor headpiece and an 11 base-pair half-operator determined by nuclear magnetic resonance spectroscopy and restrained molecular dynamics. J. Mol. Biol. **234**, 446–462
22 Slijper, M., Bonvin, A. M., Boelens, R. and Kaptein, R. (1996) Refined structure of *lac* repressor headpiece (1–56) determined by relaxation matrix calculations from 2D and 3D NOE data: change of tertiary structure upon binding to the *lac* operator. J. Mol. Biol. **259**, 761–773
23 Cadène, M. and Chait, B. T. (2000) A robust, detergent-friendly method for mass spectrometric analysis of integral membrane proteins. Anal. Chem. **72**, 5655–5658
24 Biemann, K. (1992) Mass spectrometry of peptides and proteins. Annu. Rev. Biochem. **61**, 977–1010
25 Gilbert, W. and Müller-Hill, B. (1966) Isolation of the *Lac* repressor. Proc. Natl. Acad. Sci. U.S.A. **56**, 1891–1898
26 Schnarr, M. and Maurizot, J. C. (1982) Secondary structure of the *lac* repressor headpiece: possibilities and limitations of a joint infrared and circular dichroism study. Eur. J. Biochem. **128**, 515–520
27 Schnarr, M. and Maurizot, J. C. (1982) Stability of the *lac* repressor headpiece against thermal denaturation and tryptic hydrolysis. Biochim. Biophys. Acta **702**, 155–162

28 Schnarr, M. and Maurizot, J. C. (1981) Unfolding of *lac* repressor and its proteolytic fragment by urea: headpieces stabilize the core within lac repressor. Biochemistry **20**, 6164–6169
29 Jain, R., Freund, H. G., Budzinsky, E. and Sharma, M. (1997) Radiation-induced formation of 3,4-dihydroxyphenylalanine in tyrosine-containing peptides and proteins as a function of X-irradiation dose. Bioconjugate Chem. **8**, 173–178
30 Karam, L. R., Dizdaroglu, M. and Simic, M. G. (1984) OH radical induced products of tyrosine peptides. Int. J. Radiat. Biol. **46**, 715–724
31 Huggins, T. G., Wells-Knecht, M. C., Detorie, N. A., Baynes, J. W. and Thorpe, S. (1993) Formation of *o*-tyrosine and dityrosine in proteins during radiolytic and metal-catalysed oxidation. J. Biol. Chem. **268**, 12341–12347
32 Gras, J., Sy, D., Eon, S., Charlier, M. and Spotheim-Maurizot, M. (2005) Consequences of intramolecular dityrosine formation on a DNA–protein complex: a molecular modeling study. Radiat. Phys. Chem. **72**, 271–278

Received 26 September 2006/24 January 2007; accepted 31 January 2007
Published as BJ Immediate Publication 31 January 2007, doi:10.1042/BJ20061466

33 Spotheim-Maurizot, M., Charlier, M. and Sabattier, R. (1990) DNA radiolysis by fast neutrons. Int. J. Radiat. Biol. **57**, 301–313
34 Xu, G. and Chance, M. R. (2005) Radiolytic modification and reactivity of amino acid residues serving as structural probes for protein footprinting. Anal. Chem. **77**, 4549–4555
35 Guan, J. Q. and Chance, M. R. (2005) Structural proteomics of macromolecular assemblies using oxidative footprinting and mass spectrometry. Trends Biochem. Sci. **30**, 583–592
36 Takamoto, K. G. and Chance, M. R. (2006) Radiolytic protein footprinting with mass spectrometry to probe the structure of macromolecular complexes. Annu. Rev. Biophys. Biomol. Struct. **35**, 251–276
37 Nauser, T., Koppenol, W. H. and Gebicki, J. M. (2005) The kinetics of oxidation of GSH by protein radicals. Biochem. J. **392**, 693–701
38 Boubrik, F. and Rouviere-Yaniv, J. (1995) Increased sensitivity to γ irradiation in bacteria lacking protein HU. Proc. Natl. Acad. Sci. U.S.A. **92**, 3958–3962